DOI: 10.1002/cbic.201000008

Photocontrol of Protein Activity in Cultured Cells and Zebrafish with One- and Two-Photon Illumination

Deepak Kumar Sinha,[a] Pierre Neveu,[a, b, i] Nathalie Gagey,[b] Isabelle Aujard,[b] Chouaha Benbrahim-Bouzidi,[b] Thomas Le Saux,[b] Christine Rampon,[c, d] Carole Gauron,[c] Bernard Goetz,[b] Sylvie Dubruille,[e] Marc Baaden,[f] Michel Volovitch,[c, g] David Bensimon,*[a, h] Sophie Vriz,*[c, d] and Ludovic Jullien*[b]

We have implemented a noninvasive optical method for the fast control of protein activity in a live zebrafish embryo. It relies on releasing a protein fused to a modified estrogen receptor ligand binding domain from its complex with cytoplasmic chaperones, upon the local photoactivation of a nonendogenous caged inducer. Molecular dynamics simulations were used to design cyclofen-OH, a photochemically stable inducer of the receptor specific for 4-hydroxy-tamoxifen (ER^{T2}). Cyclofen-OH was easily synthesized in two steps with good yields. At submicromolar concentrations, it activates proteins fused to the ER^{T2} receptor. This was shown in cultured cells and in zebrafish embryos through emission properties and subcellular localization of properly engineered fluorescent proteins. Cyclofen-OH was successfully caged with various photolabile protecting groups. One particular caged compound was efficient in photoinducing the nuclear translocation of fluorescent proteins either globally (with 365 nm UV illumination) or locally (with a focused UV laser or with two-photon illumination at 750 nm). The present method for photocontrol of protein activity could be used more generally to investigate important physiological processes (e.g., in embryogenesis, organ regeneration and carcinogenesis) with high spatiotemporal resolution.

Introduction

Cells respond to external signals by modifying their internal state and their environment. In multicellular organisms in particular, cellular differentiation and intracellular signaling are essential for the coordinated development of the organism.[1] Revealing and understanding the spatiotemporal dynamics of these complex interaction networks is a major goal in biology. While some of the most important players of these networks have been identified, much less is known of the quantitative rules that govern their interaction with one another and with other cellular components (affinities, rate constants, strength of nonlinearities, such as feedback or feed-forward loops, etc.). Investigating these interactions, which is a prerequisite for understanding or modeling them, requires the development of means to control or interfere spatially and temporally with these processes.

To address these issues, various approaches have been introduced to control protein activity. A first strategy relies on tuning protein concentration by controlling gene expression or messenger RNA translation. This goal can be achieved with conditional gene expression systems[2] or by using antisense oligonucleotides.[3] However, such a control introduces delays associated with mRNA or protein syntheses that prevent interference with protein patterns at the time scale of fast biological processes, such as phosphorylation.[4] A second strategy avoids this drawback by directly acting at the protein level: the activity of the protein of interest is restored with an appropriate stimulus. The fast spatiotemporal dynamics of photoactivation methods have proved particularly attractive. In favorable cases, photoactivatable substrates can be used to alter the

[a] *Dr. D. K. Sinha, Dr. P. Neveu, Dr. D. Bensimon*
Ecole Normale Supérieure
Département de Physique and Département de Biologie
Laboratoire de Physique Statistique UMR CNRS-ENS 8550
24 rue Lhomond, 75231 Paris (France)
E-mail: david.bensimon@ens.fr

[b] *Dr. P. Neveu, Dr. N. Gagey, Dr. I. Aujard, C. Benbrahim-Bouzidi, Dr. T. Le Saux, B. Goetz, Prof. Dr. L. Jullien*
Ecole Normale Supérieure, Département de Chimie
UMR CNRS-ENS-UPMC Paris 06 8640 PASTEUR
24 rue Lhomond, 75231 Paris (France)
E-mail: ludovic.jullien@ens.fr

[c] *Dr. C. Rampon, C. Gauron, Prof. Dr. M. Volovitch, Prof. Dr. S. Vriz*
Collège de France, UMR 8542 CNRS-ENS-CDF
11 place M. Berthelot, 75231 Paris Cedex 05 (France)
E-mail: vriz@univ-paris-diderot.fr

[d] *Dr. C. Rampon, Prof. Dr. S. Vriz*
Université Paris Diderot-Paris 7
80, rue du Général Leclerc Bat G. Pincus
94276 Le Kremlin-Bicêtre Cedex (France)

[e] *S. Dubruille*
Institut Curie, UMR 176 Institut Curie–CNRS
26, rue d'Ulm, 75005 Paris (France)

[f] *Dr. M. Baaden*
Institut de Biologie Physico-Chimique
Laboratoire de Biochimie Théorique, CNRS UPR 9080
13, rue Pierre et Marie Curie, 75005 Paris (France)

[g] *Prof. Dr. M. Volovitch*
Ecole Normale Supérieure, Département de Biologie
46, rue d'Ulm, 75231 Paris Cedex 05 (France)

[h] *Dr. D. Bensimon*
Department of Chemistry and Biochemistry, UCLA, Los Angeles (USA)

[i] *Dr. P. Neveu*
Kavli Institute for Theoretical Physics
University of California at Santa Barbara, Santa Barbara CA 93106 (USA)

Supporting information for this article is available on the WWW under http://dx.doi.org/10.1002/cbic.201000008.

function of native or engineered proteins.[5,6] Direct caging of peptides and proteins has been reported by many groups.[7] However, the caged precursors of these macromolecules must be injected into cells and this limits their range of access. Genetically encoded photoactivatable proteins do not suffer from this drawback in transgenic organisms. They can be designed to intrinsically bear the photoactive trigger.[8] Alternatively, they can contain a nonphotoactive site, which can be activated by a small permeant caged lipophilic molecule, such as those derived from estradiol,[9] ecdysone,[10] 4-hydroxy tamoxifen,[11,12] or doxycycline.[13] This method has been successfully implemented to photocontrol gene expression in eukaryotic systems with one- and two-photon excitation.[9,10,12,13]

In the present study, we retained the principle of a small lipophilic caged inducer to photoactivate properly engineered proteins, in vivo. We adopted a steroid-related inducer since various proteins (e.g., Engrailed, Otx2, GaL4, p53, kinases, such as Raf-1, Cre and Flp recombinases) fused to a steroid receptor have been shown to be activated by binding of an appropriate ligand (Scheme 1).[14] In its absence, the receptor forms a cytoplasmic assembly with a chaperone complex, which inactivates the fusion protein.[15] Its function is restored in the presence of the steroid ligand, which binds to the receptor and disrupts the complex. Like Link et al.,[12] we chose to photocontrol the activity of a target protein by fusing it to the extensively used modified estrogen receptor ligand binding domain, ER^{T2}, which is specific for the nonendogenous 4-hydroxy-tamoxifen inducer (tamoxifen-OH; Scheme 1).[16]

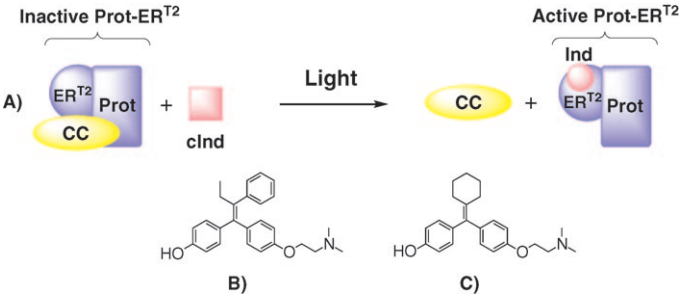

Scheme 1. A) The strategy to photoactivate properly engineered proteins. A protein fused to the ER^{T2} receptor (Prot; here a fluorescent protein linked to the receptor by a peptide acting as a nuclear localization signal) is inactivated by its assembly with a chaperone complex (CC). Upon photoactivation of a caged precursor (**cInd**), a nonendogenous inducer (**Ind**) is released and binds to the ER^{T2} moiety. The concomitant conformational change of the receptor causes assembly disruption and activates the ER^{T2}-fused protein. Examples of inducers: B) **Ind**: 4-hydroxy-tamoxifen (tamoxifen-OH), and C) 4-hydroxy-cyclofen (cyclofen-OH).

When aiming to photocontrol the activity of proteins in a live animal, the zebrafish (*Danio rerio*) is a system of choice. Its transparency and the existence of lines without pigments, its small size, easy maintenance and transgenesis, abundant progeny and rapid development allow real-time observations under the microscope. In fact, zebrafish has become a popular vertebrate model for developmental studies[17,18] and the investigation of human pathologies.[19–22] It was successfully used for large-scale genetic screens and its genomic sequence is now available and provides valuable tools.

The experimental protocol for the present photocontrol of protein activity in zebrafish is straightforward. First, an animal expressing the appropriate fusion protein is engineered (preferably permanently by incorporating the appropriate transgene in its genome or alternatively transiently by injecting its mRNA at the zygote stage). The embryo is incubated in an aqueous solution of the caged inducer that penetrates the whole organism. At a chosen stage of development, it is transferred to an illumination chamber where the inducer is uncaged in the targeted cell(s) of the animal. The released ligand then activates the protein fused to its receptor. In the present study, we report photocontrol over nuclear translocation of GFP–nls-ER^{T2} and mCherry–nls-ER^{T2}, two fluorescent proteins linked to the ER^{T2} receptor by a nuclear localization signal.

Results and Discussion

Cyclofen-OH synthesis

Since we observed that tamoxifen-OH was susceptible to photoisomerization and photodegradation upon UV illumination at uncaging time scales (see the Supporting Information) we looked for another inducer structurally related to tamoxifen-OH, but which would neither isomerize nor degrade upon UV illumination. In view of its synthetic accessibility, we were attracted by the core motif of the estrogen, cyclofenil (the bis-(acetate) of the diphenol **1** in Scheme 2).[23] In particular we wondered whether 4-hydroxy-cyclofen (cyclofen-OH or **Ind**; Scheme 1) would be as active in binding the estrogen receptor as tamoxifen-OH.

To obtain some insight about the interaction of the cyclofen-OH putative inducer with the modified estrogen receptor (ER^{T2}) we performed several molecular dynamics (MD) simulations using tamoxifen-OH as a reference. In the absence of any crystal structure of the tamoxifen-OH–ER^{T2} complex, we analyzed the interaction of both cyclofen-OH and tamoxifen-OH with the steroid receptor ERα mutated to adopt the ER^{T2} sequence (Gly400Val, Met543Ala, Leu544Ala) starting from the 2.0 Å crystal structure of the ERα ligand binding domain complexed with lasofoxifene,[24] a compound structurally closely related to tamoxifen (and tamoxifen-OH). We investigated the interaction of tamoxifen-OH and of cyclofen-OH with the reference ligand binding domain (simulations T1 and C1, respectively). We also analyzed the interaction of cyclofen-OH with the Asp351Glu mutant, in order to assess whether a slightly longer acidic side chain at position 351 might benefit binding (simulation C2).

All MD simulations lead to stable ligand binding domain–ligand complexes. Figure 1 shows representative snapshots of the three simulations. The ligands are firmly inserted in their binding pockets and are in very similar orientations for T1, C1 and C2. In particular, in the detailed view of the C1 binding pocket and ligand orientation shown in Figure 1C, the cyclofen-OH ligand positions itself in a similar way to other known ERα ligands.[24] Furthermore, the stabilization of each ligand in

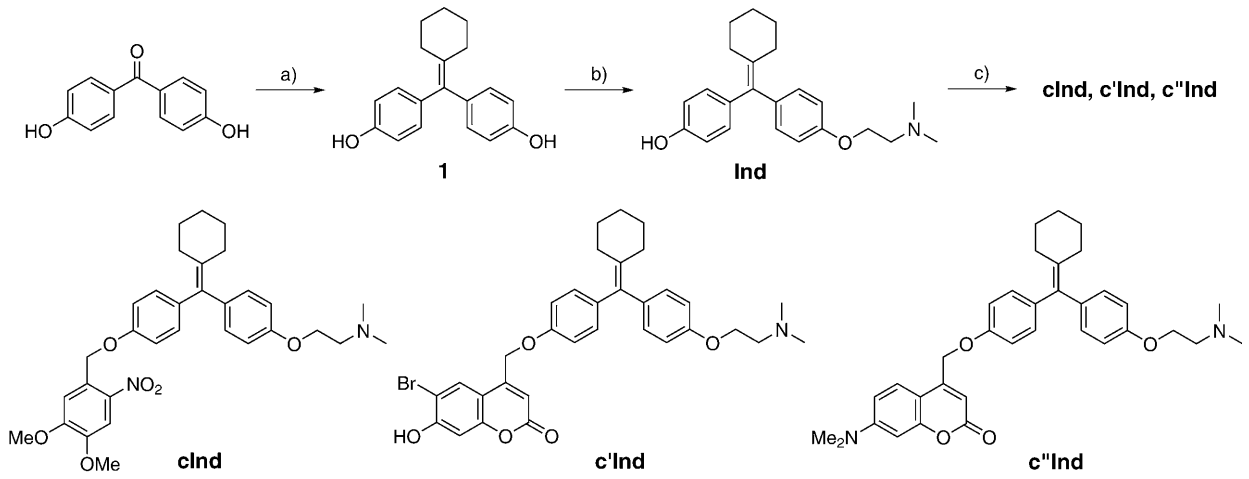

Scheme 2. Syntheses of 4-hydroxy-cyclofen (**Ind**) and its caged derivatives: a) cyclohexanone, $TiCl_4$, Zn, THF, reflux, 2 h; b) $Cl(CH_2)_2N(CH_3)_2{\cdot}HCl$, K_2CO_3, acetone/H_2O, reflux, 18 h; c) caging alcohol, $P(Ph)_3$, diisopropylazo dicarboxylate, THF, sonication, 20 min.

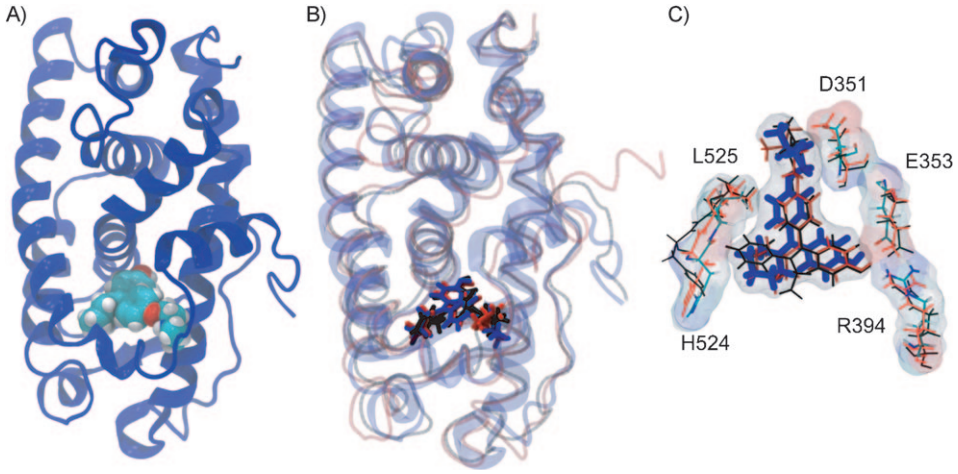

Figure 1. MD simulation snapshots. A) Representative structure of simulation C1 highlighting the position of the cyclofen-OH ligand within the ligand binding domain. The cyclofen-OH ligand remains solvent accessible through two accessibility sites: a large cleft, which could serve ligand binding and unbinding, and a channel that might enable solvent to hydrate the binding site; B) superposition of representative ligand binding domain–ligand complexes from simulations T1 (black), C1 (blue) and C2 (red). The actual values of the root mean square displacements (RMSD) of the protein stabilized beyond 20 ns are low, with C1 showing the least deviation (1.4 Å) and the reference simulation T1 was around 2 Å RMSD. The mutant C2 shows a slightly higher RMSD (2.9 Å) induced by the introduction of a longer side chain at position 351; C) zoom on the ligand binding site with key interacting residues (Arg394, Glu353, Asp351, His524, and Leu525).

complex was assessed by its contacts with the receptor (see the Supporting Information). All structural analysis, observed binding mode, number of contacts and hydrogen bonds extracted from MD simulations eventually led us to adopt cyclofen-OH as a putative ER^{T2} inducer since the ER^{T2}–cyclofen-OH complex should exhibit comparable binding properties with respect to the reference tamoxifen-OH complex.

Cyclofen-OH synthesis

Cyclofen-OH (**Ind**) was easily synthesized in two steps (Scheme 2): 4,4′-hydroxybenzophenone and cyclohexanone were first coupled under McMurry reaction conditions (85% yield)[25] and the resulting diphenol was subsequently monoalkylated with 2-(dimethylamino)ethyl chloride hydrochloride (40% yield) to provide the targeted compound. In particular, cyclofen-OH synthesis does not require any delicate separation after monoalkylation since the intermediate **1** is symmetrical. This is in contrast to tamoxifen-OH synthesis, which involves either the separation of *Z* and *E* stereoisomers or the performance of stereoselective reactions.[26]

Validation of the cyclofen-OH inducer

First, we tested cyclofen-OH in CV1 cells transfected with a plasmid expressing the *gfp–nls-ER*^{T2} fusion gene. When observed by epifluorescence microscopy 24 h later, these cells displayed a weak cytoplasmic fluorescence background with occasional nuclear fluorescence (Figure 2A). Addition of cyclofen-OH (or tamoxifen-OH) to the cell culture medium resulted in the disappearance of cytoplasmic fluorescence and a strong increase in nuclear fluorescence without alteration of the cell morphology (Figure 2B). As expected, the release upon ligand binding of GFP–nls-ER^{T2} from its cytoplasmic chaperone complex permitted its nuclear translocation. We measured the cumulative distribution of nuclear fluorescence intensities (Figure 2C) from which we extracted the average values (Figure 2D; see the Experimental Section). In the absence of ligand, that probability differed significantly from zero only at low fluorescence intensities. Upon addition

of cyclofen-OH, the fraction of cells displaying strong nuclear fluorescence increased with the concentration of ligand and yielded a larger average value. Noticeably, the data revealed that cyclofen-OH and tamoxifen-OH induced similar fluorescence distributions at 3 μM of ligand (Figure 2C), a similarity expected from the MD simulations of their binding to the ER^{T2} receptor. Thus, it appears that cyclofen-OH is nontoxic and as efficient as tamoxifen-OH in binding to the ER^{T2} receptor of the GFP–nls-ER^{T2} fusion protein and in activating its nuclear translocation.

We then checked whether zebrafish embryos developed normally when incubated in various concentrations of cyclofen-OH (up to 5 μM) and displayed a similar response to cell cultures when GFP–nls-ER^{T2} (or mCherry–nls-ER^{T2}) mRNA was injected (at the one-cell stage). In the absence of ligand, the embryos displayed a very weak, overall fluorescence signal at 30 h postfertilization (hpf; Figure 3A and at dome stage in Figure S3A in the Supporting Information). Upon incubation in a medium containing the ligand, the percentage of positive embryos (defined as those exhibiting nuclear fluorescence at 24 hpf) increased (Figure 3B and Figure S3B in the Supporting Information) reaching 50% at an inducer concentration, $C_{1/2} = 0.2$ μM (Figure 3C and Table S2 in the Supporting Information).

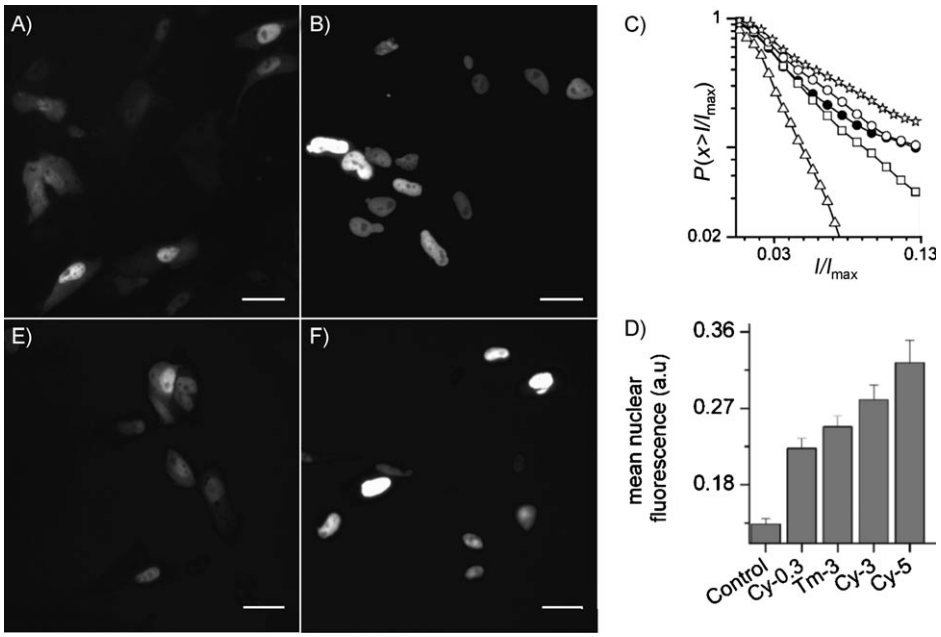

Figure 2. Induction of nuclear translocation of GFP–nls-ER^{T2} by addition or photorelease of cyclofen-OH in CV1 cells transfected with gfp–nls-ER^{T2} plasmid. GFP fluorescence image of CV1 cells 24 h after transfection and further incubation with: A) 0, or B) 3 μM **Ind** for 1 h (identical display range in A and B). C) Cumulative distribution after 0.0 (△), 0.3 (□), 3.0 (○) and 5.0 μM (☆) **Ind**, or 3.0 μM (●) tamoxifen-OH treatment. D) Average value of the mean nuclear intensity; error bars represent standard errors of the mean. GFP fluorescence image of CV1 cells imaged 24 h after transfection and further incubation in 6 μM **cInd** for 30 min, E) without, and F) with global 365 nm UV illumination; scale bar: 10 μm.

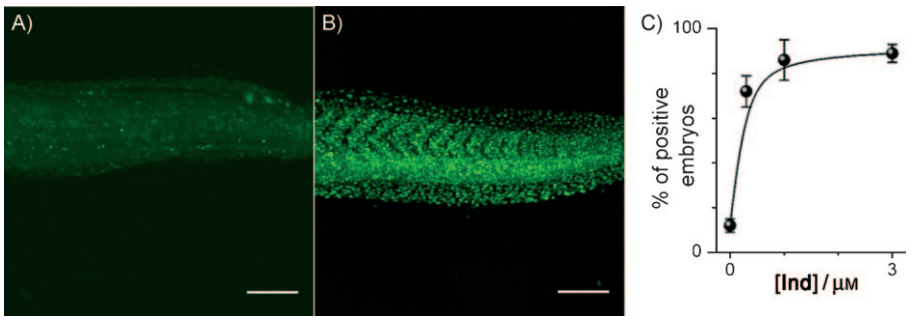

Figure 3. Induction of nuclear translocation of GFP–nls-ER^{T2} by addition of cyclofen-OH in wild-type zebrafish embryos injected with *gfp–nls-ER^{T2}* mRNA (100 ng μL^{-1}) at the one-cell stage. GFP fluorescence image of embryos at 24–30 hpf after incubation with: A) 0, or B) 3 μM **Ind**. Note that the camera sensitivity was intensified by a factor of 6 in A) with respect to B). C) Dependence of the efficiency of nuclear translocation of GFP–nls-ER^{T2} on inducer concentration. Error bars are statistical errors estimated as $\sqrt{(p(1-p)/n)}$, where p is the percentage of embryos exhibiting a positive phenotype, and n is the total number of embryos investigated. The solid line is a guide for the eyes; scale bar: 100 μm.

Caged cyclofen-OH: syntheses and in vitro photochemical properties

Following the validation of cyclofen-OH as an efficient ER^{T2} ligand and its possible use to control protein activity in cell cultures and zebrafish embryos, we caged it with 4,5-dimethoxy-2-nitrobenzyl alcohol, 6-bromo-7-hydroxy-4-hydroxymethyl-coumarin[27] and 7-dimethyl-amino-4-hydroxymethyl-coumarin[28] under Mitsonobu conditions to give **cInd**, **c′Ind**, and **c″Ind** with 64, 45, and 32% yields, respectively (Scheme 2).

We characterized the uncaging of these compounds, in vitro, using HPLC coupled to mass spectrometry to measure the temporal dependence of the concentration of photoreleased cyclofen-OH. With UV illumination at 365 nm, we observed that the inducer **Ind** could be photoreleased quantitatively from its three caged precursors **cInd**, **c′Ind**, and **c″Ind** with characteristic times of 270, 120, and 620 s, respectively, corresponding to uncaging cross-sections with one-photon excitation at 365 nm of 22, 47, and 10 M^{-1} cm^{-1} (see the Supporting Information). We found that the **cInd** and **c″Ind** caged precursors were inert in the dark and led to photocontrol in zebrafish embryos upon UV illumination. In contrast, **c′Ind** led to protein activation in zebrafish embryos, even in the absence of

illumination. In the following we will focus on the easily accessible **cInd**. We showed that cyclofen-OH could be released from **cInd** with two-photon illumination at 750 nm with an uncaging cross-section equal to 4 mGM (see the Supporting Information) in agreement with values reported for the photolabile 4,5-dimethoxy-2-nitrobenzyl protecting group.[27,29] Although modest, this uncaging cross-section is sufficient to achieve **cInd** uncaging at the 10 s time scale in a cell volume at nondetrimental laser powers (10–20 mW with our 40× microscope objective; see the Supporting Information).

Caged cyclofen-OH induced protein photoactivation in cells

In the absence of UV illumination, the fluorescence of CV1 cells transfected with a plasmid carrying a *gfp–nls-ER^{T2}* fusion gene incubated in 6 μM **cInd** for 30 min was essentially the same as that observed in cells incubated without inducer (compare Figure 2A and E). This result shows that the caged ligand **cInd** was inactive and nontoxic. On the other hand, when **cInd** was illuminated by UV for a duration similar to its uncaging time, the cells displayed the characteristic nuclear fluorescence they show in the presence of ligand (compare Figure 2B and F).

We also used short light pulses emitted by a 365 nm UV laser or by a Ti-Sa laser at 750 nm in a nondetrimental[30] power regime (5 s at 5 μW and 10 s at 10–20 mW at the sample) to photorelease **Ind** and analyze the translocation kinetics of GFP–nls-ER^{T2} in a single cell with one- and two-photon excitation, respectively. In all cases, the cytoplasm and the nucleus of the targeted illuminated cell exhibited much faster brightness changes than surrounding cells: they become dimmer and brighter, respectively. This behavior is evidenced in Figure 4A and B by comparing the fluorescence levels in the cytoplasm and in the nucleus of the targeted cell by using the nearby unilluminated cell as a reference. Figure 4C shows that the average nuclear fluorescence intensity of a targeted cell increases exponentially with time, leading to an estimate of the nuclear translocation time $\tau_{int} = (1000 \pm 300)$ s. In contrast, at the same time scale, the fluorescence level remains fairly constant in the reference cell as well as in a control experiment in which a cell not incubated with **cInd** was submitted to the same laser exposure (wavelength, power and duration) as in the targeted cell in Figure 4A.

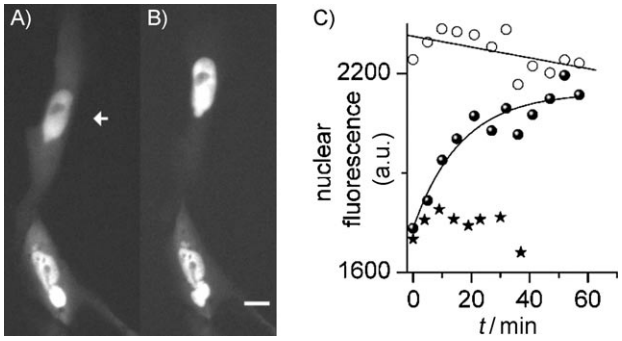

Figure 4. Selective nuclear GFP–nls-ER^{T2} translocation in one CV1 cell (indicated by an arrow in A) upon two-photon illumination (750 nm, 10 mW for 10 s). Fluorescence images of the targeted cell and a nearby unilluminated cell: A) 0, and B) 60 min after illumination. C) Time evolution of the mean nuclear fluorescence intensity in the targeted cell (●) and the reference cell (○) shown in A) and B). The stars depict the corresponding evolution for a **cInd** nonincubated control cells, which were illuminated similarly to the targeted cell in A). The CV1 cells were transfected with a gfp–nls-ER^{T2} plasmid, further incubated in 6 μM **cInd** for 30 min and washed before illumination; scale bar: 10 μm.

We eventually studied the kinetics of translocation from the fluorescence correlation spectroscopy (FCS) signal of the cytoplasmic GFP–nls-ER^{T2}. We recorded time-series of FCS curves following uncaging of **cInd** (6 μM) in targeted cells (Figure S6 in the Supporting Information). The FCS curves have been globally analyzed as a function of the time (t) after cyclofen-OH release by adopting a model in which the illumination volume is assumed to contain two fluorescent species with diffusion constant D_i ($i = 1, 2$): a GFP–nls-ER^{T2} unbound state **1** and a chaperone bound complex **2**.[31] The FCS curve can then be written as [Eq. (1)]:

$$G(\tau) = \sum_{i=1}^{2} \left(\frac{Q_i \overline{N_i}}{\sum_{i=1}^{2} Q_i \overline{N_i}} \right)^2 G_i(\tau, N_i, \tau_i) \quad (1)$$

with [Eq. (2)]:

$$G_i(\tau, N_i, \tau_i) = \frac{1}{\overline{N_i}} \left(1 + \frac{\tau}{\tau_i}\right)^{-1} \left(1 + \omega^2 \frac{\tau}{\tau_i}\right)^{-\frac{1}{2}} \quad (2)$$

where $\overline{N_i}$ is the average number of molecules in state i, contained in the illumination volume, Q_i and τ_i ($= \omega_{xy}^2/4D_i$) their brightness and diffusion time through the beam waist (ω_{xy}) and $\omega = \omega_z/\omega_{xy}$ the aspect ratio of the illuminated volume. Satisfactory fits were obtained with various (τ_1,τ_2) combinations without significantly altering characteristic decay times. To reduce uncertainties, we fixed $\tau_i = 1.7$ ms, a value contained in the range allowed by the previous fits and derived for GFP–nls-ER^{T2} from the GFP diffusion coefficient (25 μm^2 s^{-1})[32] by taking into account the difference of molecular weights (66.6 kDa for GFP–nls-ER^{T2} and 27 kDa for GFP).[33] Then we performed a satisfactory global fit of the whole series of FCS autocorrelation curves (Figure S6 in the Supporting Information). From these fits the values of [Eq. (3)]:

$$G_i(\tau = 0, t) = \frac{Q_i^2 \overline{N_i}(t)}{\left(Q_1 \overline{N_1}(t) + Q_2 \overline{N_2}(t)\right)^2} \quad (3)$$

at various times (t) were determined. It turns out that the ratio $G_1(0,t)/G_2(0,t)$ is constant (Figure 5A), which implies that the ratio of bound to unbound species is also constant. We thus deduced that the equilibrium between these two states occurs on a time scale faster than the one associated to nuclear translocation. We correspondingly observed similar characteristic times associated to the exponential increase of $G_i(0,t)$ (Figure 5B and C). From $G_1(0,t) + G_2(0,t)$, which is inversely proportional to the number of cytoplasmic GFP–nls-ER^{T2} molecules, we eventually deduced that nuclear translocation happens on a timescale $t_n = (450 \pm 20)$ s (Figure 5D) that is in the same order of magnitude as the value deduced from the increase in nuclear fluorescence and in line with published estimates.[34]

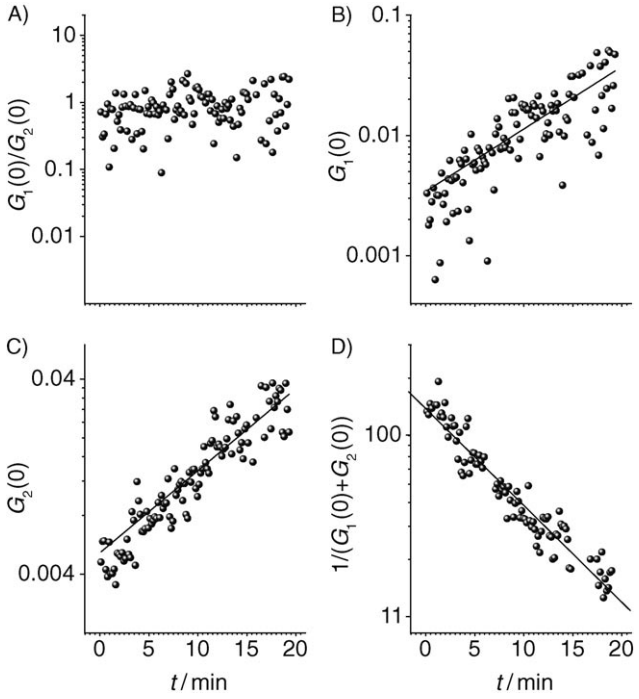

Figure 5. Analysis of the FCS autocorrelation curves of cytoplasmic GFP in a CV1 cell transfected with a gfp–nls-ER^{T2} plasmid, incubated in 6 μM **cInd** for 30 min and illuminated for 5 s with a UV laser (375 nm, 5 μW; see also Figure S6 in the Supporting Information). Time dependence of: A) $G_1(\tau=0,t)/G_2(\tau=0,t)$, B) $G_1(\tau=0,t)$, C) $G_2(\tau=0,t)$, and D) $1/[G_1(\tau=0,t)+G_2(\tau=0,t)]$ extracted from a two-species model with $\tau_1=1.7$ ms and $\tau_2=240$ ms. Dots: experimental points; solid line: fit to an exponential decrease of the cytoplasmic species (due to nuclear translocation).

Caged cyclofen-OH-induced protein photoactivation in zebrafish embryos

We then investigated the photoinduction of nuclear translocation in live zebrafish embryos. Wild-type embryos were injected with *gfp–nls-ER^{T2}* mRNA at the one-cell stage and incubated (at 1 to 2 hpf) for 90 min in embryo medium supplemented with 3 μM **cInd**. As observed in cell cultures, **cInd** was inactive and nontoxic. In comparison with embryos incubated in regular medium, it did not induce a significantly larger GFP nuclear translocation and mortality (Figure 6A and Table S3 in the Supporting Information).

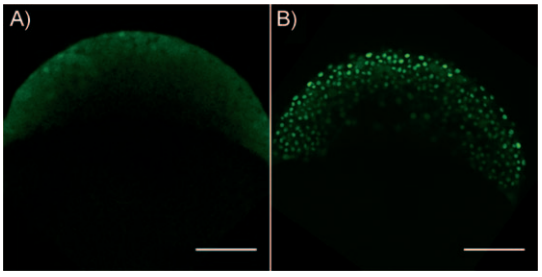

Figure 6. Induction of nuclear translocation of GFP–nls-ER^{T2} by photorelease of cyclofen-OH in wild-type zebrafish embryos injected with *gfp–nls-ER^{T2}* mRNA (100 ng μL^{-1}) at the one-cell stage. Confocal GFP fluorescence image of embryos at 4 hpf (following incubation at 2 hpf for 90 min in 3 μM **cInd** and washing): A) without illumination, and B) 30 min after illumination with UV light; scale bar: 100 μm.

Upon uncaging of **cInd** by UV illumination of the whole embryo at 4–5 hpf, a global nuclear translocation of the GFP-fused protein was observed, in line with the cell culture data (Figure 6B). We studied the dependence of GFP nuclear translocation on the duration of UV illumination in more detail (Table S3 and Figure S5 in the Supporting Information). As anticipated, the translocation yield increased with illumination duration. Using the dependence observed in Figure 3C for calibration, the data also suggested that the concentration of **cInd** in the embryo was in the same range as its concentration in the incubation solution (see the Supporting Information).

Then, to verify that the photocontrol of protein activity did locally occur around targeted illuminated cells, we performed a colocalization experiment involving two caged compounds sharing the same caging group: **cInd** and caged fluorescein dextran (**cFd**). We used a UV laser (5 μW) to perform a local photoactivation (for 5 s) of **cInd** and **cFd** in wild-type embryos injected at the one-cell stage with **cFd** and *gfp–nls-ER^{T2}* mRNA and incubated in embryo medium supplemented with 3 μM **cInd**. From the different emission spectra of GFP and fluorescein, their contributions to the fluorescence signal were separated by analyzing images recorded at different wavelengths. Figure 7A–C displays images of a zebrafish embryo (60 min after illumination) that were obtained from recording the emission from GFP, fluorescein, and both fluorophores, respectively. One notices the cytoplasmic localization of fluorescein in the group of cells in which the GFP–nls-ER^{T2} signal is predominantly localized in the nucleus.

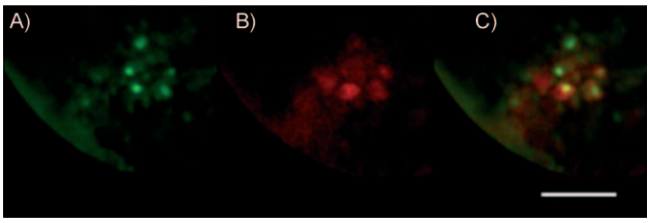

Figure 7. Images resulting from local photoactivation of GFP–nls-ER^{T2} in a wild-type embryo injected with *gfp–nls-ER^{T2}* mRNA and caged fluorescein dextran at the one-cell stage and conditioned as in Figure 6A and B. Emission from: A) GFP, B) fluorescein, and C) both fluorophores; scale bar: 100 μm.

We also performed a second colocalization experiment with two-photon illumination. Our aim here was to demonstrate the colocalization of the two fluorescent proteins, GFP–nls-ER^{T2} and mCherry–nls-ER^{T2}, the latter acts as a reporter of the illuminated cell. Figure 8A–C displays the distribution of fluorescence intensity in a wild-type embryo injected with *gfp–nls-ER^{T2}* and *mCherry–nls-ER^{T2}* mRNA at the one-cell stage. After incubation from the dome stage to 24 hpf in embryo medium supplemented with 3 μM **cInd** and subsequent washing, the embryo was illuminated at 24 hpf in the tail for 10 s with a Ti-Sa laser (750 nm, 10 mW). After 60 min, we observed a marked increase in fluorescence from a single nucleus in both green and red fluorescence channels, indicating that nuclear translocation of both GFP–nls-ER^{T2} and mCherry–nls-ER^{T2} occurred in

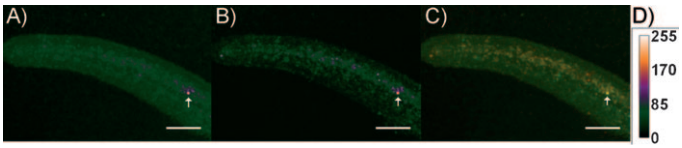

Figure 8. Images resulting from local photoactivation (750 nm, 10 mW, 10 s) of GFP–nls-ER^{T2} and mCherry–nls-ER^{T2} in the tail at 24 hpf in a wild-type embryo. A) GFP, and B) mCherry, and C) their superposition evidences the colocalization of these proteins after photoactivation; D) the images are intensity coded; scale bar: 100 μm.

a single cell of the embryo. To rule out the possibility that observing a bright spot was due to statistical variation rather than photoactivation, we performed a statistical analysis on the distributions of fluorescence intensity from GFP–nls-ER^{T2} and mCherry–nls-ER^{T2} in the images of the fish tail displayed in Figure 8 A and B (see the Supporting Information). As shown in Figure S7 in the Supporting Information, both normalized histograms of fluorescence levels exhibit a smooth distribution at low fluorescence intensity, corresponding to the population of background cells and therefore acting as an internal control, and a spike at much higher intensity associated to the bright cell. From the intensity distributions, we computed their mean (μ_g,μ_r) and standard deviations (σ_g,σ_r) and noticed that the intensity of the green and red fluorescence signal in the bright cell was observed at 16.7 σ_g and 10.6 σ_r, respectively, from the distribution means. From these observations, we estimate that the probability of observing a random fluctuation of fluorescence in both channels is smaller than $\exp(-50) \sim 10^{-22}$, which is negligibly small, even after multiplying by the number of cells in the tail. We thus deduce that this highly localized fluorescence of both GFP–nls-ER^{T2} and mCherry–nls-ER^{T2} in the nucleus of a single cell results from the local two-photon uncaging of **cInd**, which was indeed performed in the area where we observed this increased localized fluorescence 60 min later under a confocal microscope.

Conclusions

We have shown that photoreleasing cyclofen-OH from a caged precursor is an efficient strategy to restore the function of a protein fused to the ER^{T2} receptor and investigated its dynamical effects in cultured cells and in live zebrafish embryos. Colocalization experiments, with both UV and two-photon excitations, suggest that the light-induced activation of proteins can be restricted to a small group of targeted cells. This observation is significant when evaluating the feasibility of the photocontrol of protein activity down to the single cell level by using the present approach. From the data of the cyclofen-OH dose-response curve, the kinetics of uncaging and an estimate of the cyclofen-OH concentration within the embryo, one can set the two-photon illumination conditions to deliver and tune the concentration of cyclofen-OH in the targeted cell to a level slightly below the saturation of its receptor. Any leakage of the inducer in the extracellular medium and the neighboring cells would then be at too low a concentration to turn on protein activity in those cells. The present noninvasive optical method is compatible with a wide variety of proteins and could open up opportunities for the local spatiotemporal investigation of developmental pathways,[35,36] the identification of stem cells and the study of cancer in a live organism.

Experimental Section

Molecular dynamics simulation: MD simulations were run for 30 ns with the YASARA program.[37] Force-field parameterization for tamoxifen-OH and cyclofen-OH ligands was carried out by using the AutoSMILES procedure, otherwise the AMBER99 forcefield was used.[38] All systems were solvated with 7936 explicit TIP3P water molecules and 20 Na^+ and 22 Cl^- counterions were added as background salt and to preserve overall electrical neutrality. Each system was energy minimized by using the steepest descent method to relax any steric conflicts before beginning the simulations. Simulations were carried out with periodic boundary conditions. Long-range electrostatic interactions were calculated by using PME with a direct-space cut-off of 7.86 Å. All simulations were performed by using an NVT ensemble at 298 K. A 2 fs/1 fs double-integration time step was used. Graphics were prepared with VMD.[39] Standard conformational analysis was carried out by using YASARA, Gromacs tools[40] and locally written code. Statistical and data analysis was performed by using the R statistical software package[41] and Xmgrace.[42]

Syntheses

General: 4,5-Dimethoxy-2-nitrobenzyl alcohol was purchased from Sigma. 6-Bromo-7-hydroxy-4-hydroxymethyl-coumarin and 7-dimethylamino-4-hydroxymethylcoumarin were synthesized according to published procedures.[43,44] Commercially available reagents were used as obtained. Microanalyses were performed by the Service de Microanalyses de Gif sur Yvette. Melting points were determined with a Büchi 510 capillary apparatus. The ^1H and ^{13}C NMR spectra were recorded at room temperature on Bruker AM 250 or 400 spectrometers; chemical shifts are reported in ppm with protonated solvent as internal reference (^1H, $CHCl_3$ in $CDCl_3$ 7.26 ppm, CHD_2OD in CD_3OD 3.31 ppm, CHD_2SOCD_3 in CD_3SOCD_3 2.49 ppm, CHD_2COCD_3 in CD_3COCD_3 2.05 ppm; ^{13}C, $^{13}CDCl_3$ in $CDCl_3$ 77.0, $^{13}CD_3OD$ in CD_3OD 49.1 ppm, $^{13}CD_3SOCD_3$ in CD_3SOCD_3 39.7 ppm, $^{13}CD_3COCD_3$ in CD_3COCD_3 29.9 ppm); coupling constants (*J*) are given in Hz. Mass spectra (chemical ionization and high resolution with NH_3 or CH_4) were performed by the Service de Spectrométrie de Masse de l'ENS (Paris). Column chromatography was performed on silica gel 60 (0.040–0.063 nm; Merck). Analytical thin-layer chromatography (TLC) was conducted on Merck silica gel 60 F_{254} precoated plates. HPLC analyses and purifications of the final caged species were performed on a Waters system incorporating a Wdelta 600 pump with a PDA 996 UV detector working at 245 nm (columns: analytical: X-Terra Waters MS C18, 150×4.6 mm, 5 μm, 1 mL min^{-1} flow; preparative: X-Terra Waters Prep MS C18, 150×19 mm, 5 μm, 12 mL min^{-1} flow; elution with solution A: water with 0.05% formic acid; and solution B: acetonitrile with 0.05% formic acid).

*4-(Cyclohexylidene(4-hydroxyphenyl)methyl)phenol (**1**):*[25] Titanium chloride (6.2 mL, 56 mmol) was added dropwise under argon to a stirred suspension of zinc powder (8.20 g, 126 mmol) in dry tetrahydrofuran (80 mL) at −10 °C. When the addition was complete, the mixture was warmed to room temperature and then refluxed for 2 h. A solution of 4,4′-hydroxybenzophenone (2.0 g, 9 mmol) and cyclohexanone (4 mL, 38 mmol) in dry tetrahydrofuran (120 mL) was added to the cooled suspension of the titanium re-

agent at 0 °C and the mixture was refluxed for 2 h. After being cooled to room temperature, the reaction mixture was quenched with 10% (*w/v*) aqueous potassium carbonate (30 mL), filtered and extracted with ethyl acetate. The organic layer was washed with brine, dried over $MgSO_4$, and concentrated in vacuo. Flash column chromatography (cyclohexane/ethyl acetate, 3:1, *v/v*) afforded **1** as a white powder (2.15 g, 85%). ^{1}H NMR (250 MHz, [D_6]DMSO): δ = 9.28 (s, 2H), 6.82 (d, J = 8.4 Hz, 4H), 6.65 (d, J = 8.4 Hz, 4H), 2.14 (m, 4H), 1.52 (m, 6H); ^{13}C NMR (100 MHz, [D_6]DMSO): δ = 155.5, 136.2, 133.8, 133.6, 130.3, 114.6, 31.9, 28.1, 26.3.

*4-((4-(2-(Dimethylamino)ethoxy)phenyl)(cyclohexylidene)methyl)-phenol (**Ind**; 4-hydroxy-cyclofen):* 2-(Dimethylamino)ethylchloride hydrochloride (256 mg, 1.78 mmol) was dissolved in a solution of acetone/water (19:1 *v/v*, 40 mL) and treated with potassium carbonate (600 mg, 4.4 mmol). The mixture was stirred at 0 °C for 30 min. Compound **1** (500 mg, 1.78 mmol) was dissolved in the above solution at 0 °C and potassium carbonate (580 mg, 4.2 mmol) was added. The mixture was refluxed for 18 h. The solids were filtered off, and the filtrate was concentrated in vacuo. The crude product was purified by flash column chromatography (dichloromethane/methanol, 9:1, *v/v*) to afford **Ind** as a white powder (250 mg, 40%). m.p.: 180–181 °C (methanol); ^{1}H NMR (250 MHz, $CDCl_3$): δ = 6.95–6.89 (m, 4H), 6.70 (AA′XX′, J = 8.5 Hz, 2H), 6.59 (AA′XX′, J = 8.5 Hz, 2H), 4.04 (t, J = 5.5 Hz, 2H), 2.82 (t, J = 5.5 Hz, 2H), 2.40 (s, 6H), 2.25–2.21 (m, 4H), 1.57 (m, 6H); ^{13}C NMR (100 MHz, $CDCl_3$): δ = 156.6, 154.7, 137.9, 136.1, 135.0, 133.5, 131.0, 130.8, 115.0, 113.5, 64.6, 58.1, 45.3, 45.2, 32.5, 32.4, 28.6, 26.8; MS (CI, CH_4): *m/z* 352 (calcd average mass for $C_{23}H_{29}NO_2$: 351.22); MS (CI, CH_4, HR): *m/z* 352.2271 (calcd average mass for $C_{23}H_{30}NO_2$: 352.2277); elemental analysis calcd (%) for $C_{23}H_{29}NO_2 \cdot 0.5\,H_2O$ (360.49): C 76.63, H 8.39, N 3.89; found: C 76.95, H 8.09, N 3.87.

2-(4-((4-(4,5-Dimethoxy-2-nitrobenzyloxy)phenyl)cyclohexylidene)methyl)phenoxy)-N,N-*dimethylethanamine (**cInd**):*[45] A solution of **Ind** (180 mg, 0.5 mmol), 4,5-dimethoxy-2-nitrobenzyl alcohol (115 mg, 0.54 mmol) and triphenylphosphine (140 mg, 0.54 mmol) in tetrahydrofuran (0.25 mL) was sonicated for several minutes to allow for mixing. Diisopropylazodicarboxylate (0.106 mL, 0.54 mmol) was added dropwise to the resulting viscous solution during sonication. After sonicating for 20 min, the reaction mixture was concentrated in vacuo and purified by column chromatography on silica gel with dichloromethane/methanol (9:1, *v/v*) as eluent to give **cInd** (180 mg, 64%); m.p.: 116–117 °C (isopropylether, yellow crystals); ^{1}H NMR (400 MHz, $CDCl_3$): δ = 7.76 (s, 1H), 7.35 (s, 1H), 7.04 (AA′XX′, J = 8.7 Hz, 2H), 7.00 (AA′XX′, J = 8.7 Hz, 2H), 6.90 (AA′XX′, J = 8.7 Hz, 2H), 6.82 (AA′XX′, J = 8.7 Hz, 2H), 5.47 (s, 2H), 4.03 (t, J = 5.8 Hz, 2H), 3.96 (s, 3H), 3.94 (s, 3H), 2.70 (t, J = 5.8 Hz, 2H), 2.32 (s, 6H), 2.23 (m, 4H), 1.58 (m, 6H); ^{13}C NMR (100 MHz, $CDCl_3$): δ = 157.0, 156.2, 153.8, 147.7, 138.9, 138.5, 136.8, 137.7, 133.2, 131.0, 130.7, 129.6, 114.3, 113.8, 109.4, 107.9, 67.0, 65.8, 58.3, 56.3, 56.3, 45.8, 32.4, 28.6, 26.8; elemental analysis calcd (%) for $C_{32}H_{38}N_2O_6$ (546.66): C 70.32, H 7.00, N 5.12; found: C 70.11, H 7.24, N 5.02. After preparative HPLC purification (elution profile: 0–5 min: 50% A and 50% B; 5–15 min: 10% A and 90% B), **cInd** was shown by analytical HPLC to contain less than 2% residual of **Ind**.

*4-((4-((4-(2-(Dimethylamino)ethoxy)phenyl)(cyclohexylidene)methyl)-phenoxy)methyl)-6-bromo-7-hydroxycoumarin (**c′Ind**):* This was obtained in the same way as **cInd** by using **Ind** (110 mg, 0.31 mmol), 6-bromo-7-methoxymethoxy-4-hydroxycoumarin[46] (100 mg, 0.31 mmol), triphenylphosphine (86 mg, 0.33 mmol), diisopropylazodicarboxylate (0.065 mL, 0.33 mmol) and tetrahydrofuran (0.2 mL). After sonication, trifluoroacetic acid (2 mL) was added and the mixture was stirred at room temperature for 15 min. The solvent was removed in vacuo. Purification by column chromatography with dichloromethane/methanol (9:1, *v/v*) as eluent yielded **c′Ind** (60 mg, 30%). ^{1}H NMR (250 MHz, [D_6]DMSO): δ = 8.00 (s, 1H), 7.09–6.75 (m, 9H), 6.39 (s, 1H), 5.33 (s, 2H), 4.06 (t, J = 5.6 Hz, 2H), 2.75 (t, J = 5.6 Hz, 2H), 2.32 (s, 6H), 2.17 (m, 4H), 1.55 (s, 6H); ^{13}C NMR (100 MHz, $CDCl_3$): δ = 160.2, 157.0, 156.2, 155.8, 154.1, 149.1, 138.7, 137.3, 135.6, 133.0, 131.0, 130.7, 127.5, 114.1, 113.8, 112.6, 111.9, 108.4, 104.0, 65.7, 65.5, 58.1, 45.7, 32.4, 28.6, 26.7; MS (CI, NH_3): *m/z* 606.604 (calcd average mass for $C_{33}H_{35}{}^{81}BrNO_5$: 606.19, $C_{33}H_{35}{}^{79}BrNO_5$: 604.16); MS (CI, NH_3, HR): *m/z* 606.1677 (calcd average mass for $C_{33}H_{35}{}^{81}BrNO_5$: 606.1684), 604.1693 (calcd average mass for $C_{33}H_{35}{}^{79}BrNO_5$: 604.1699). After preparative HPLC purification (elution profile: 0–5 min: 50% A and 50% B; 5–15 min: 10% A and 90% B), **c′Ind** was shown by analytical HPLC to contain less than 2% residual of **Ind**.

*4-((4-((4-(2-(Dimethylamino)ethoxy)phenyl)(cyclohexylidene)methyl)-phenoxy)methyl)-7-dimethylaminocoumarin (**c″Ind**):* This was obtained in the same way as **cInd** by using **Ind** (200 mg, 0.57 mmol), 7-(dimethylamino)-4-(hydroxymethyl)-2*H*-chromen-2-one[44] (125 mg, 0.57 mmol), triphenylphosphine (150 mg, 0.57 mmol), diisopropylazodicarboxylate (0.112 mL, 0.57 mmol) and tetrahydrofuran (0.3 mL). Purification by column chromatography with dichloromethane/methanol (9:1, *v/v*) as eluent, yielded **c″Ind** (100 mg, 32%). ^{1}H NMR (250 MHz, $CDCl_3$): δ = 7.38 (d, J = 8.9 Hz, 1H), 7.04–6.74 (m, 8H), 6.61 (dd, J = 2.4, 8.9 Hz, 1H), 6.53 (d, J = 2.4 Hz, 1H), 6.32 (s, 1H), 5.12 (s, 2H), 4.15 (t, J = 5.2 Hz, 2H), 3.05 (s, 6H), 2.91 (t, J = 5.2 Hz, 2H), 2.48 (s, 6H), 2.22 (m, 4H), 1.57 (m, 6H); ^{13}C NMR (63 MHz, $CDCl_3$): δ = 161.9, 157.0, 156.2, 156.0, 152.8, 150.5, 138.6, 137.0, 135.8, 133.2, 131.0, 130.9, 124.3, 114.1, 113.9, 108.9, 107.7, 106.8, 98.4, 65.9, 65.7, 58.2, 45.7, 40.1, 32.5, 28.6, 26.8; MS (CI, CH_4): *m/z* 553 (calcd average mass for $C_{35}H_{41}N_2O_4$: 553.3; MS (CI, CH_4, HR): *m/z* 553.3065 (calcd average mass for $C_{35}H_{41}N_2O_4$: 553.3066). After preparative HPLC purification (elution profile: 0–50 min: 15% A and 85% B), **c″Ind** was shown by analytical HPLC to contain less than 2% residual of **Ind**.

HPLC coupled to mass spectrometry: High pressure liquid chromatography was carried out with an Accela system liquid chromatograph (Thermo Finnigan, Les Ulis, France) equipped with a Hypersil gold column (1.9 μm × 2.1 × 50 mm) connected to a Thermo-Finnigan TSQ Quantum Discovery Max triple quadrupole mass spectrometer. Sample solution (5 μL) was injected in the chromatographic column. For photodeprotection studies, the samples were eluted in isocratic mode at a flow rate of 400 μL min^{-1} with a water/acetonitrile mixture (60–40%, *v/v*) containing 0.05% formic acid. For the isomerization study, the separation of isomers was carried out by gradient elution at a flow rate of 400 μL min^{-1} from 5% to 95% water/methanol mixtures containing 0.05% formic acid in 20 min. Between each injection, the column was equilibrated with the mobile phase for 5 min. After separation, the analytes were introduced in the mass spectrometer through a heated electrospray ionization source (50 °C) operating in the positive mode. The temperature of the capillary transfer was set at 270 °C. Nitrogen was employed as nebulizing (35 psi) and auxiliary gas (30 arbitrary units). Argon was used as collision gas (1.0 milliTorr in Q2). 4-Hydroxy-cyclofen (**Ind**) was observed (ion spray voltage of 3000 V) in the single reaction monitoring (SRM) mode (*m/z* 352.2 → 72) by using 30 V collision energy and 130 V tube lens. The stereoisomers of 4-hydroxytamoxifen and the corresponding dehydrophenanthrens (ion spray voltage of 3000 V) were followed in the single ion monitoring (*m/z* 388.3) mode by using 175 V tube lens. All the possible settings were optimized by repetitive injections of the analyte in the chromatographic system. Instrument control and data col-

lection were handled by a computer equipped with Xcalibur software (version 2.0).

Methods for experiments in cells and zebrafish embryos

Application of the inducers and their caged precursors: Tamoxifen-OH, cyclofen-OH (**Ind**) and its various caged precursors (**cInd**, **c′Ind**, **c″Ind**) were solubilized at 10 mM in DMSO; these stock solutions were stored at −20 °C and proved stable for several months. Aliquots of those solutions were added to the aqueous solutions containing the cells and the zebrafish embryos to reach the concentrations indicated in the text. The dilution factor exceeded 10^3 and we did not notice any effect when the same volume of pure DMSO was added to the biological samples in control experiments. After incubation with the caged precursors, the cells and the zebrafish embryos were washed with plain medium prior to illumination to avoid any possible interference, which could originate from photoreleasing the inducer in the incubating solution.

The gfp–nls-ER^{T2} and mCherry–nls-ER^{T2} coding plasmids: An intermediate vector (pC5fiERT) was first constructed by inserting Cre-ER^{T2} coding sequence (fragment XhoI–EcL136I from pCre-ER^{T2},[47] a kind gift from Daniel Metzger and Pierre Chambon, Strasbourg, France) into pcDNA5/FRT (Invitrogen, digested with XhoI and EcoO109I, blunted with Klenow). We then prepared pC5fGFPERT, which contained the *gfp–nls-ER^{T2}* coding sequence downstream of the CMV and T7 promoters and upstream the bovine growth hormone polyadenylation signal, by trimolecular ligation between the NheI–BsrGI fragment from pEGFP-C1 (Invitrogen), pC5fiERT cleaved by NheI and XhoI, and a BsrGI–XhoI adaptor (sense: 5′-GTA CAG GAT CCC CAA GAA GAA GCG CAA GGT GGC GCC CGG GC-3′; antisense: 5′-TCG AGC CCG GGC GCC ACC TTG CGC TTC TTC TTG GGG ATC CT-3′). The pC5fGFPERT plasmid codes for a 567 amino acid (aa) long fusion protein (1–238: eGFP[aa1–aa238]; 239–253: RIP-SV40nls-APGLEP; 254–567: hESR1[aa282–aa595, with three mutations G400V, M543A, L544A]). This construct was used for expression in CV1 cells, and a second plasmid was built by transferring the NheI–PmeI fragment of pC5fGFPERT into pCS2+ (a kind gift from Richard M. Harland, Berkeley, California, cleaved by XbaI and SnaBI). The new construct, pCSGFPnERT, which contained the same *gfp–nls-ER^{T2}* coding sequence downstream simian CMV and SP6 promoters and upstream the late SV40 polyadenylation signal, was used to prepare synthetic RNA in vitro for injection into zebrafish embryos. Plasmid pCSmChnERT was obtained by substituting mCherry for the GFP sequence, through insertion of the BamHI–SgrAI fragment of pREST-mCherry (a kind gift from Roger Y. Tsien,[48] San Diego, California) into pCSnERT (a derivative of pCSGFPnERT prepared by inserting an adaptor between BamHI and SmaI sites; sense: 5′-GAT CCTA GGC TAG CAC CGG CGG CAT GGA CGA GCT GCT GTA CAA ATC GAT CCC CAA GAA GAA GCG CAA GGT GGC GCC C-3′, antisense: 5′-GGG CGC CAC CTT GCG CTT CTT CTT GGG GAT CGA TTT GTA CAG CAG CTC GTC CAT GCC GCC GGT GCT AGC CTA G-3′) cleaved by BamHI and SgrAI. The pCSmChnERT plasmid codes for a 566 aa long fusion protein (1–237: mCherry[aa1–aa237]; 238–252: SIP-SV40nls-APGLEP; 253–566: hESR1[aa282–aa595, with three mutations G400V, M543A, L544A]). All conditions for restriction digests, gel purification, ligation and bacteria transformation were according to standard procedures.[49] Complete plasmid sequences are available upon request.

Cell experiments: CV1 cells were plated on 35 mm Petri dishes in 1 to 2 mL of incubation medium (10% FBS in DMEM) at a density of 100–200 cells per mm^2 and incubated at 37 °C and 5% CO_2 for 24 h before transfection. CV1 cells were transfected with plasmid (1 μg) by using Lipofectamin (Invitrogen). To assay the effect of the various ligands or their caged precursors, CV1 cells were incubated at various concentrations of these substrates (0–5 μM) for different durations (15–60 min) and fixed in PFA (4%) before imaging. In uncaging assays of **cInd**, the molecule was added 24 hpt for 15 to 30 min before illumination. Expression of GFP–nls-ER^{T2} was assayed 24 h after transfection by imaging the GFP fluorescence.

Zebrafish embryo experiments: Wild-type zebrafish embryos were injected at the one-cell stage with the appropriate mRNA synthesized with an in vitro transcription kit (mMessage mMachine, Ambion). They were subsequently dechorionated by pronase treatment at dome stage prior to incubation in an aqueous solution of the various substrates (up to 30 hpf with **Ind**, for 90 min with **cInd** except for the experiment displayed in Figure 8, which was up to 24 hpf). **Ind** was photoreleased from **cInd** 4–5 hpf (except in Figure 8, 24 hpf). Illuminated embryos were observed 30 min (60 min in Figure 8) after illumination for GFP–nls-ER^{T2} or mCherry–nls-ER^{T2} fluorescence. Embryos positive for either GFP or mCherry nuclear translocation were scored under a microscope in a double-blind protocol.

Image acquisition and analysis: A fluorescence microscope (Olympus BX51WI) equipped with a Luca CCD Camera (Andor technologies) was used for image acquisition of the cells (filters: U-MWIBA3 Olympus for GFP and U-MWIG3 Olympus for mCherry). In a given series of experiments, all the conditions (EM gain, exposure duration, lamp power, etc.) were identical to allow for a comparison of the observed fluorescence intensities. The images of embryos were acquired by using confocal microscopes Leica TCS SP2 AOBS or Zeiss Axiovert 200M LSM510-Meta. To obtain Figure 2C and D, we analyzed the images recorded at all the **Ind** concentrations by extracting the average nuclear intensity (I) from each cell (at least 100 cells were analyzed at each **Ind** concentration) with a home-developed LabView program by using IMAQ VISION (a rectangular region of interest (roi) was manually drawn across each cell in each image. The IMAQ AutoBThreshold vi (virtual instrument: LabView program) was then used to compute the optimal threshold value for each roi—with a single cell inside a roi—to segment the nuclear region from the rest. We subsequently plotted the resulting histogram I/I_{max} after normalization relative to the intensity I_{max} of the brightest cell nucleus across all the cells and all the **Ind** concentrations. At a given **Ind** concentration, the cumulative distribution function $P(x>I/I_{max})$, which represents the probability that the random variable I/I_{max} takes on a value less than or equal to x, was subsequently obtained by integrating the histogram from 0 to I/I_{max} and normalizing such that $P(x>0)=1$ (Figure 2C). Averaging the histogram was correspondingly performed to extract the averaged values shown in Figure 2D. For the analysis of the phenotypes resulting in Figure 3C and Figure S5 in the Supporting Information, we considered as positive those embryos exhibiting a spotty fluorescence associated to fluorescence localized in the nuclei. For the analysis of localization and colocalization of GFP and fluorescein displayed in Figure 7A–C, we performed multichannel fluorescence imaging (excitation: 488 nm; emission channels: 500–512, 512–522 and 530–600 nm). Using reference spectra acquired from embryos labeled with GFP or fluorescein only, and assuming the total measured fluorescence in any channel to linearly reflect the individual contributions of the fluorophores, we used a home-written Matlab code to retrieve the fractional intensities of GFP and fluorescein.

Fluorescence correlation spectroscopy: FCS was used: 1) to characterize the focal points of the various objectives by analyzing the autocorrelation curves of 50 or 100 nM fluorescein solutions in 0.1 M NaOH (V_{exc}, the illuminated volume, from the value of the

autocorrelation function at zero time by using fluorescein concentration and ω_{xy}, the beam waist, from the fluorescein diffusion time by using its known diffusion coefficient);[50] 2) to analyze the kinetics of the nuclear translocation of GFP–nls-ER^{T2}. For FCS experiments, illumination in the preceding microscope (Olympus BX51WI) was provided either by a 488 nm laser (Ar-ion, Spectra Physics) or by a mode-locked Ti-Sapphire laser (200 fs, 76 MHz, 750 nm; Mira, Coherent). The fluorescence photons were collected through filters (U-MWIBA3 set; without excitation filter, emission filter: BP460–495), dichroic mirrors (DM505 for 488 nm excitation and 700 short pass; Olympus for 750 nm excitation wavelengths) and optical fibers (FG200 LCR multimode fiber, Thorlabs) and were detected with avalanche photodiodes (SPCM-AQR-14, Perkin–Elmer) coupled to an ALV-6000 correlator (ALV GmbH). The incident powers at the sample were measured with a NOVA II powermeter (Laser Measurement Instruments). All the series of experiments reported in the present work were performed in a regime of laser powers (3 to 5 μW for 488 nm and 5 to 20 mW for 750 nm) in which fluorescein exhibits a linear (with one-photon excitation) or quadratic (with two-photon excitation) dependence of the intensity of fluorescence emission on the illumination power.

Illumination experiments

UV lamps: One-photon illumination experiments were performed at 20 °C, with bench top UV lamps (365 nm, essentially a strong line at 365 nm accompanied by a Gaussian spectral dispersion around 350 nm with a 40 nm width at half height; Fisher Bioblock) delivering typical 2.2×10^{-5} (4 W; in vitro experiments) and 4×10^{-5} (6 W; in vivo experiments) Einstein min^{-1} photon fluxes in the illuminated sample.[6] We found that when illuminated for up to 4 min the embryos developed normally. We also verified that the byproduct resulting from uncaging **cInd** did not induce any noticeable morphological alterations in embryo development.

UV laser and two-photon excitation: A 40×0.8 NA water immersion objective (Olympus) was used to image the embryos on a CCD camera (Andor Luca) and locate the focal spot of the UV laser/two-photon excitation. For the UV illumination (375 nm, CW, from Crystal Laser) a beam of 1 mm diameter was coupled to the microscope without expansion. For two-photon illumination (200 fs, 76 MHz, 750 nm, provided by a mode-locked Ti-Sapphire laser, Mira, Coherent) the beam was expanded to ~6 mm diameter to fill the back aperture of the objective. The incident power at the sample (~5 μW with the UV and ≥20 mW with the IR laser) was measured with a NOVA II powermeter (Laser Measurement Instruments).

Acknowledgements

This work has been supported by the ANR (PCV 2008, Proteophane), the NABI CNRS–Weizmann Institute program (fellowship to D.K.S.), and the Ministère de la Recherche (fellowships to N.G. and P.N.). P.N. is supported in part by the National Science Foundation under grant no. PHY05-51164. D.B. acknowledges partial support of a PUF ENS-UCLA grant. M.B. thanks ANR for support (Project ANR-06-PCVI-0025). The authors thank Philippe Leclerc and Benjamin Matthieu for their kind help with confocal imaging. They are also thankful to Dr. Vincent Jullien and Prof. Gérard Pons at Service de Pharmacologie Clinique, Saint Vincent de Paul Hospital Paris, for access to their HPLC-MS instrument. The authors thank Dr. Daniel Metzger (IGBMC, Strasbourg, France) for providing the original plasmid containing the ER^{T2} coding sequence. Gil Levkowitz is acknowledged for a generous gift of caged fluorescein dextran. The authors declare no competing financial interests.

Keywords: cage compounds · cells · gene expression · photochemical methods · protein modifications

[1] J. Gerhart, M. Kirschner, *Cells, Embryos, and Evolution*, Blackwell, Malden, MA, **1997**.
[2] A. D. S. Ryding, M. G. F. Sharp, J. J. Mullins, *J. Endocrinol.* **2001**, *171*, 1–14.
[3] S. Karkare, D. Bhatnagar, *Appl. Microbiol. Biotechnol.* **2006**, *71*, 575–586.
[4] a) A. Fujioka, K. Terai, R. E. Itoh, K. Aoki, T. Nakamura, S. Kuroda, E. Nishida, M. Matsuda, *J. Biol. Chem.* **2006**, *281*, 8917–8926; b) J. Dengjel, V. Akimov, J. V. Olsen, J. Bunkenborg, M. Mann, B. Blagoev, J. S. Andersen, *Nat. Biotechnol.* **2007**, *25*, 566–568.
[5] M. Volgraf, P. Gorostiza, R. Numano, R. H. Kramer, E. Y. Isacoff, D. Trauner, *Nat. Chem. Biol.* **2006**, *2*, 47–52.
[6] P. Neveu, I. Aujard, C. Benbrahim, T. Le Saux, J.-F. Allemand, S. Vriz, D. Bensimon, L. Jullien, *Angew. Chem.* **2008**, *120*, 3804–3806; *Angew. Chem. Int. Ed.* **2008**, *47*, 3744–3746.
[7] a) *Dynamic Studies in Biology* (Eds.: M. Goeldner, R. Givens), Wiley-VCH, Weinheim, **2005**; b) G. Mayer, A. Heckel, *Angew. Chem.* **2006**, *118*, 5020–5042; *Angew. Chem. Int. Ed.* **2006**, *45*, 4900–4921; c) G. C. R. Ellis-Davies, *Nat. Methods* **2007**, *4*, 619–628; d) H.-M. Lee, D. R. Larson, D. S. Lawrence, *ACS Chem. Biol.* **2009**, *4*, 409–427; e) A. Specht, F. Bolze, Z. Omran, J.-F. Nicoud, M. Goeldner, *HFSP J.* **2009**, *3*, 255–264.
[8] a) F. Zhang, L.-P. Wang, M. Brauner, J. F. Liewald, K. Kay, N. Watzke, P. G. Wood, E. Bamberg, G. Nagel, A. Gottschalk, K. Deisseroth, *Nature* **2007**, *446*, 633–641; b) Y. I. Wu, D. Frey, O. I. Lungu, A. Jaehrig, I. Schlichting, B. Kuhlman, K. M. Hahn, *Nature* **2009**, *461*, 104–108.
[9] F. G. Cruz, J. T. Koh, K. H. Link, *J. Am. Chem. Soc.* **2000**, *122*, 8777–8778.
[10] W. Y. Lin, C. Albanese, R. G. Pestell, D. S. Lawrence, *Chem. Biol.* **2002**, *9*, 1347–1353.
[11] Y. Shi, J. T. Koh, *ChemBioChem* **2004**, *5*, 788–796.
[12] K. H. Link, Y. Shi, J. T. Koh, *J. Am. Chem. Soc.* **2005**, *127*, 13088–13089.
[13] S. B. Cambridge, D. Geissler, F. Calegari, K. Anastassiadis, M. T. Hasan, A. F. Stewart, W. B. Huttner, V. Hagen, T. Bonhoeffer, *Nat. Methods* **2009**, *6*, 527–533.
[14] D. Picard, *Curr. Opin. Biotechnol.* **1994**, *5*, 511–515.
[15] a) J. Cheung, D. F. Smith, *Mol. Endocrinol.* **2000**, *14*, 939–946; b) D. Picard, *Trends Endocrinol. Metabol.* **2006**, *17*, 229–235; c) W. B. Pratt, Y. Morishima, Y. Osawa, *J. Biol. Chem.* **2008**, *283*, 22885–22889.
[16] a) R. Feil, J. Brocard, B. Mascrez, M. LeMeur, D. Metzger, P. Chambon, *Proc. Natl. Acad. Sci. USA* **1996**, *93*, 10887–10890; b) J. Brocard, X. Warot, O. Wendling, N. Messaddeq, J.-L. Vonesch, P. Chambon, D. Metzger, *Proc. Natl. Acad. Sci. USA* **1997**, *94*, 14559–14563.
[17] R. T. Peterson, B. A. Link, J. E. Dowling, S. L. Schreiber, *Proc. Natl. Acad. Sci. USA* **2000**, *97*, 12965–12969.
[18] P. J. Keller, A. D. Schmidt, J. Wittbrodt, E. H. K. Stelzer, *Science* **2008**, *322*, 1065–1069.
[19] J. T. Shin, M. M. C. Fishman, *Annu. Rev. Genomics Hum. Genet.* **2002**, *3*, 311–340.
[20] U. Langheinrich, *BioEssays* **2003**, *25*, 904–912.
[21] G. E. Ackermann, B. H. Paw, *Front. Biosci.* **2003**, *8*, 1227–1253.
[22] J. F. Amatruda, J. L. Shepard, H. M. Stern, L. I. Zon, *Cancer Cell* **2002**, *1*, 229–231.
[23] C. B. Lunan, A. Klopper, *Clin. Endocrinol.* **1975**, *4*, 551–572.
[24] F. F. Vajdos, L. R. Hoth, K. F. Geoghegan, S. P. Simons, P. K. LeMotte, D. E. Danley, M. J. Ammirati, J. Pandit, *Protein Sci.* **2007**, *16*, 897–905.
[25] M. M. Cid, J. A. Seijas, M. C. Villaverde, L. Castedo, *Tetrahedron* **1988**, *44*, 6197–6200.
[26] S. Gauthier, J. Mailhot, F. Labrie, *J. Org. Chem.* **1996**, *61*, 3890–3893.
[27] T. Furuta, S. S.-H. Wang, J. L. Dantzker, T. M. Dore, W. J. Bybee, E. M. Callaway, W. Denk, R. Y. Tsien, *Proc. Natl. Acad. Sci. USA* **1999**, *96*, 1193–1200.

[28] V. R. Shembekar, Y. Chen, B. K. Carpenter, G. P. Hess, *Biochemistry* **2005**, *44*, 7107 – 7114.
[29] a) E. B. Brown, J. B. Shear, S. R. Adams, R. Y. Tsien, W. W. Webb, *Biophys. J.* **1999**, *76*, 489 – 499; b) I. Aujard, C. Benbrahim, M. Gouget, O. Ruel, J. B. Baudin, P. Neveu, L. Jullien, *Chem. Eur. J.* **2006**, *12*, 6865 – 6879.
[30] We mentioned the possible photoinduced damage arising in biological samples when two-photon illumination is used for photoactivation (see page seven of the Supporting Information of ref. [6]). In the present work, we paid attention to remain in the nondetrimental regime of laser powers.
[31] In all investigated cases, a global fit of the FCS curves to a one-species diffusion model was poor.
[32] Y. Chen, J. D. Müller, Q. Q. Ruan, E. Gratton, *Biophys. J.* **2002**, *82*, 133 – 144.
[33] From the diffusion times $\tau_1 = 1.7$ ms and $\tau_2 = 240$ ms, we deduced the corresponding diffusion coefficients for the unbound and bound species: $D_1 = 18.5\ \mu m^2 s^{-1}$ and $D_2 = 0.1\ \mu m^2 s^{-1}$. In particular, D_2 is significantly smaller than D_1 as anticipated from the formation of a large complex between GFP–nls-ER^{T2} and the chaperone complex.
[34] a) N. Shulga, P. Roberts, Z. Gu, L. Spitz, M. M. Tabb, M. Nomura, D. S. Goldfarb, *J. Cell. Biol.* **1996**, *135*, 329 – 339; b) R. B. Kopito, M. Elbaum, *Proc. Natl. Acad. Sci. USA* **2007**, *104*, 12743 – 12748.
[35] I. A. Shestopalov, J. K. Chen, *Chem. Soc. Rev.* **2008**, *37*, 1294 – 1307.
[36] P. Neveu, D. Sinha, P. Kettunen, S. Vriz, L. Jullien, D. Bensimon in *Single Molecule Spectroscopy in Chemistry, Physics and Biology* (Eds.: A. Gräslund, R. Rigler, J. Widengren), Springer, Heidelberg, **2009**, pp. 305 – 316.
[37] E. Krieger, T. Darden, S. B. Nabuurs, A. Finkelstein, G. Vriend, *Proteins Struct. Funct. Bioinf.* **2004**, *57*, 678 – 683.
[38] J. Wang, P. Cieplak, P. A. Kollman, *J. Comput. Chem.* **2000**, *21*, 1049 – 1074.
[39] W. Humphrey, A. Dalke, K. Schulten, *J. Mol. Graph.* **1996**, *14*, 33 – 38.
[40] GROMACS (http://www.gromacs.org).
[41] R Development Core Team, R: *A Language and Environment for Statistical Computing*, Vienna, Austria, **2007**.
[42] Grace (http://plasma-gate.weizmann.ac.il/Grace/).
[43] H. J. Montgomery, B. Perdicakis, D. Fishlock, G. A. Lajoie, E. Jervis, J. G. Guillemette, *Bioorg. Med. Chem.* **2002**, *10*, 1919 – 1927.
[44] T. Eckardt, V. Hagen, B. Schade, R. Schmidt, C. Schweitzer, J. Bendig, *J. Org. Chem.* **2002**, *67*, 703 – 710.
[45] S. D. Lepore, Y. He, *J. Org. Chem.* **2003**, *68*, 8261 – 8263.
[46] A. Z. Suzuki, T. Watanabe, M. Kawamoto, K. Nishiyama, H. Yamashita, M. Ishii, M. Iwamura, T. Furuta, *Org. Lett.* **2003**, *5*, 4867 – 4870.
[47] R. Feil, J. Wagner, D. Metzger, P. Chambon, *Biochem. Biophys. Res. Commun.* **1997**, *237*, 752 – 757.
[48] N. C. Shaner, R. E. Campbell, P. A. Steinbach, B. N. G. Giepmans, A. E. Palmer, R. Y. Tsien, *Nat. Biotechnol.* **2004**, *22*, 1567 – 1572.
[49] J. M. Urbach, T. Wei, N. Liberati, D. Grenfell-Lee, J. Villanueva, G. Wu, F. M. Ausubel, *Curr. Protoc. Mol. Biol.* **2009**, Unit 19.7.
[50] O. Krichevsky, G. Bonnet, *Rep. Prog. Phys.* **2002**, *65*, 251 – 297.

Received: January 5, 2010
Published online on February 24, 2010

